CONDUCTING (Si-DOPED) ALUMINUM NITRIDE EPITAXIAL FILMS GROWN BY MOLECULAR BEAM EPITAXY: EXPERIMENT AND THEORY

By

JONGJIN G. KIM

A DISSERTATION PRESENTED TO THE GRADUATE SCHOOL OF
THE UNIVERSITY OF FLORIDA IN PARTIAL FULFILLMENT
OF THE REQUIREMENTS FOR THE DEGREE
OF DOCTOR OF PHILOSOPHY

UNIVERSITY OF FLORIDA

1998

TO MY PARENTS

ACKNOWLEDGMENTS

I would like to express my deepest appreciation to Prof. Robert M. Park, my supervisory committee chairman, for his constant professional guidance, support and encouragement during the course of my research and the writing of this dissertation. I also would like to thank Prof. Rolf E. Hummel, Prof. Rajiv K. Singh, Prof. Joseph H. Simmons, and Prof. Sheng S. Li, who kindly served on my dissertation committee.

I extend my thanks to Madhu Moorthy and Lynn Calhoun, my fellow graduate students, whose valuable assistance and discussions regarding this research are gratefully acknowledged. I also would like to thank Dr. Margaret Puga, who performed the SIMS measurements for this work.

Finally, special thanks goes to my parents, and my brother and sisters (Peter, Agnes, and Katherine), whose love and support during the course of my studies I will never forget.

TABLE OF CONTENTS

Page

ACKNOWLEDGMENTS ---------- iii

ABSTRACT ---------- vi

CHAPTERS

1 INTRODUCTION ---------- 1

Background Review ---------- 1
    Critical Aspects Associated with AlGaN Epitaxial Growth ---------- 2
        1 Candidate substrates and preparation techniques ---------- 2
        2 Sapphire nitridation and buffer layer growth ---------- 4
        3 Doping of AlGaN (experiment and theory) ---------- 5
Dissertation Outline ---------- 8

2 MBE GROWTH SYSTEM AND CHARACTERIZATION TECHNIQUES -- 10

Introduction ---------- 10
MBE System ---------- 10
    Overall System Configuration ---------- 10
    Effusion Cells for Al, Ga, and Si ---------- 16
    Nitrogen Source ---------- 20
    Substrate Temperature Calibration ---------- 24
Characterization Techniques ---------- 27
    Atomic Force Microscope (AFM) ---------- 27
    Hall-effect Measurements ---------- 29
    Secondary Ion Mass Spectrometry (SIMS) ---------- 30
    High Resolution X-ray Diffraction (HRXRD) ---------- 30
    Cross-sectional Scanning Electron Microscope (SEM) ---------- 32
    Electron Microprobe ---------- 32

3 SUBSTRATE PREPARATION AND CHARACTERIZATION ---------- 34

Sapphire Substrates ---------- 34
Surface Cleaning ---------- 34

    Solvent Cleaning ---------- 34
    Chemical Polishing (etching) ---------- 37
    In situ Thermal Cleaning ---------- 47

4 SAPPHIRE NITRIDATION AND III-V NITRIDE EPILAYER GROWTH ---------- 54

Sapphire Nitridation ---------- 54
    RHEED Analysis ---------- 54
    AFM Analysis ---------- 61
    Hall-effect Measurements ---------- 61
AlN Buffer Layer Growth ---------- 67
    RHEED Analysis ---------- 68
    AFM Analysis ---------- 71
Undoped AlGaN Epilayer Growth ---------- 71
    Undoped AlN Epilayer Growth ---------- 74
    Undoped AlGaN Epilayer Growth ---------- 75

5 Si-DOPING OF HIGH Al-CONTENT AlGaN ---------- 77

Experimental Results ---------- 77
    Influence of Growth Temperature ---------- 77
    Influence of GaN Buffer Layer ---------- 79
    Influence of the Presence of a Ga Flux ---------- 84
Theoretical Model ---------- 90
    Thermodynamic Consideration ---------- 90
    Kinetic Considerations ---------- 102

6 SUMMARY AND CONCLUSIONS ---------- 108

LIST OF REFERENCES ---------- 111

BIOGRAPHICAL SKETCH ---------- 114

Abstract of Dissertation Presented to the Graduate School
of the University of Florida in Partial Fulfillment of the
Requirements for the Degree of Doctor of Philosophy

CONDUCTING (Si-DOPED) ALUMINUM NITRIDE EPITAXIAL FILMS GROWN BY MOLECULAR BEAM EPITAXY : EXPERIMENT AND THEORY

BY

Jongin George Kim

August, 1998

Chairman : Dr. Robert M. Park
Major Department : Materials Science and Engineering

As a member of the III-V nitride semiconductor family, AlN, which has a direct energy gap of 6.2eV, has received much attention as a promising material for many applications. However, despite the promising attributes of AlN for various semiconductor devices, research on AlN has been limited and conducting AlN has not been reported.

The objective of this research was to understand the factors impacting the conductivity of AlN (or high Al content AlGaN) and to control the conductivity of this material through intentional doping.

Prior to the intentional doping study, growth of undoped AlN and high Al content AlGaN epilayers was investigated. Through careful selection of substrate preparation methods and growth parameters, relatively low temperature molecular beam epitaxial growth of AlN and high Al content AlGaN films was established which resulted in insulating material.

Intentional Si doping during epilayer growth was found to result in conducting films under specific growth conditions. Above a growth temperature of 900°C AlN films were insulating, however, below a growth temperature of 900°C the AlN films were conducting.

The magnitude of the conductivity and the growth temperature range over which conducting AlN films could be grown were strongly influenced by the presence of a Ga flux during growth. For instance, conducting, Si-doped, AlN films were grown at a growth temperature of 940°C in the presence of a Ga flux while the films were insulating when grown in the absence of a Ga flux at this particular growth temperature. Also by appropriate selection of the growth parameters AlN epilayers with conductivity values as large as 17 $\Omega^{-1}\text{cm}^{-1}$ were grown in this work for the first time.

The roles of both growth temperature and Ga adatoms in controlling the conductivity of Si-doped AlN epitaxial films were considered in a model involving non-equilibrium thermodynamics and kinetics and the model was applied to explain the novel experimental observations.

CHAPTER 1
INTRODUCTION

Background Review

Research on the III-V nitride materials system (AlN, GaN, InN, and their ternaries) has been one of the hottest issues in current materials research. Ever since the successful fabrication of the first highly efficient blue light-emitting diodes[1] and blue-diode lasers,[2] enormous attention has been given to the III-V nitrides. The III-V nitride materials are not only good candidates for optoelectronic devices, but also promising materials for high temperature, high frequency, and high power electronic device applications.[3,4,5,6]

Among the III-V nitrides, AlN has recently drawn attention due to its potential for use in many device application areas. AlN displays high thermal conductivity, high temperature stability and a large direct band gap of 6.2eV and has attractive piezoelectric properties which render it suitable for surface acoustic wave device applications.[7] AlN (and high Al content AlGaN) is also of particular interest due to its negative electron affinity[8] which can be exploited for cold cathode applications in high power vacuum electronics and flat panel displays.

Despite these promising attributes, however, progress in the development of AlN-based devices has been limited due to difficulties encountered in doping the material.

Attempts to dope AlN have been made by several researchers,[9-11] however all of these attempts have resulted in the production of highly resistive material ($\rho > 1000\ \Omega$-cm)

Critical Aspects Associated with AlGaN Epitaxial Growth

1. Candidate substrates and preparation techniques

Two substrate materials have been most widely used for the growth of epitaxial $Al_xGa_{1-x}N$ namely (0001) sapphire[11] and 6-H SiC.[12] The crystalline properties of sapphire and 6H-SiC are compared with those of AlN and GaN in Table 1-1. Although, 6H-SiC is indicated to be more closely lattice matched to the $Al_xGa_{1-x}N$ system than sapphire, sapphire is considerably cheaper than 6H-SiC and in addition, sapphire surfaces can be readily nitrided prior to the epitaxial growth of III-V nitride compounds.

Sapphire is an insulating material with a bandgap of 9.5eV.[13] For surface preparation of this substrate solvent cleaning followed by chemical etching with phosphoric acid (H_3PO_4) or a mixture of 3:1 H_2SO_4:H_3PO_4 at elevated temperature (160°C) is generally used.[14,15] Such preparation is believed to eliminate impurities and the polishing damage. However, a systematic study of this chemical preparation method has not been presented in the literature. Despite the importance of the substrate surface for epitaxial growth, most studies have focused on nitridation and buffer layer growth rather than on sapphire surface preparation. *In situ* heating of the sapphire surface prior to nitridation has become a standard procedure that is believed to result in the desorption of surface contaminants.[16] Streaky reflection high energy electron diffraction (RHEED) patterns with Kikuchi bands have been reported following an *in situ* heat treatment.[17]

Crystalline properties		GaN	AlN	Sapphire	6H SiC
Lattice parameter	a	3.186	3.1114	4.758	3.081
	c	5.178	4.9792	12.991	15.092
	c/a	1.6252	1.6003	2.730	1.633 (x3)
Thermal expansion Coefficient ($\times 10^{-6}C^{-1}$)	a	5.59	4.2	7.5	4.2
	c	3.17	5.3	8.5	4.68
Interplanar distances	Basal	2.59	2.49	2.165	2.516
	(1100)	2.760	2.695	1.374	2.669
	$(11\bar{2}0)$	1.593	1.556	2.379	1.541
Lattice mismatch with	Al_2O_3	14.8%	12.5%	------	11.5%
	SiC	3.3%	1.0%	-11.5%	------
	GaN	------	-2.4%	-14.8%	-3.3%

Table 1-1 Crystalline properties of GaN, AlN, Sapphire, and 6-H SiC

Analysis of sapphire surface structures was performed before the importance of nitride growth on this material emerged.[17, 18,19,20] The low energy electron diffraction (LEED) technique was used to study the c-plane sapphire surface at different temperatures. Three main ordered structures have been observed in vacuum at different conditions (mainly temperature). A basic (1x1) structure is maintained up to 900°C where upon a $(\sqrt{3}x\sqrt{3})$ reconstructed surface develops which is rotated by 30°. Further heating changes the pattern to $(\sqrt{31}x\sqrt{31})$ rotated ± 9° above 1400°C.[17,18]

2. Sapphire nitridation and buffer layer growth

Nitridation of the sapphire surface is the process of forming an AlN layer on top of the sapphire substrate by exposing it to an active nitrogen flux. The orientation relationship has been given as (0001)//(0001) and $(11\bar{2}0)//(10\bar{1}0)$ (sapphire//AlN) which suggests that the AlN crystal is rotated by 30° in the plane with reference to the underlying sapphire crystal. From the previous section it is noted that a 30° rotation of the surface Al atom arrangement occurs in a certain temperature range (900 – 1400°C).[18] It is expected that this temperature range will be optimum for nitridation. Yeadon *et al*[6] have performed a nitridation study using NH_3 as a nitrogen source. These authors showed that the sapphire surface roughness increases with NH_3 exposure. Although it is undesirable to have a rough substrate surface since it will hinder 2-D planar growth, the AlN buffer layers grown on top of the sapphire had a better morphology. It is believed that the formation of a sufficiently nitrided surface is perhaps more important than the provision of a smooth starting surface.

III-V nitride heteroepitaxy typically involves the growth of a buffer layer. For GaN growth on sapphire, both GaN and AlN grown at low temperatures have been used as buffer layers. Low temperature (400~600°C) deposition of GaN or AlN followed by annealing (at 800°C or higher) has mostly been used.[21,22] However during low temperature deposition the buffer layer materials are amorphous and crystallize only during the annealing step. The resulting buffer layer structure is misoriented by <3° relative to the substrate and contains low-angle grain boundaries.[23] The surface is rough compared to the nitrided sapphire surface and a 3-D to 2-D transition occurs during epilayer growth on such buffer layers.

From the above concerns, it appears that relatively high temperature AlN buffer layer growth (i.e. crystalline deposition) would be more desirable for subsequent $Al_xGa_{1-x}N$ growth on sapphire.

3. Doping of AlGaN (experiment and theory)

Transparent undoped AlN single crystals have resistivities reportedly in the range, 10^{11} - 10^{13} Ω-cm.[24,25] However, it has also been reported that impure crystals, which exhibit a bluish color, possibly due to the presence of Al_2OC, have lower resistivities (10^3 - 10^5 Ω-cm).[24,25] These impure crystals were p-type and Hall-effect measurements produced very rough estimates of the AlN hole mobility ($\mu_p \approx 14$ cm^{2}V^{-1}s^{-1}). Chu *et al*[9] were able to obtain both n- and p-type AlN by introducing Hg and Se respectively. However, the resistivity of their material was too high to allow the net carrier concentrations to be determined. Rutz[26] reported a growth method which resulted in highly-resistive ($\rho \approx 10^{3}\ \Omega$ cm) n-type AlN. However the source of the electrons in this material was not determined.

With regard to more recent work, a Ge-doping study of $Al_xGa_{1-x}N$ grown on (0001) sapphire and (111) Si substrates by MOCVD has been reported.[10] In that work, H_2 diluted germane (GeH_4) was used as the dopant source and trimethylgallium (TMGa), trimethylaluminum (TMAl) and ammonia (NH_3) were used as Ga, Al, and N source, respectively. The whole range of $Al_xGa_{1-x}N$ ($0 \leq x \leq 1$) films was studied using both optical (photo-absorption and photoluminescence) and electrical (Hall-effect measurements) analyses and it was found that for x values greater than 0.2, the films were insulating while n-type material was produced for $x \leq 0.2$. N-type $Al_xGe_{1-x}N$ (for x values up to 0.42) has been achieved using SiH_4 as the dopant source in the case of MOCVD growth on 6H-SiC substrates,[1] however, $Al_xGa_{1-x}N$ films with x values greater than 0.42 were insulating. Both of the above mentioned Ge and Si doping studies employed hydrogen gas and hydrogen and/or carbon-containing source materials. Abernathy *et al.*[27] have studied the impact of carbon and hydrogen incorporation on III-V nitrides. Hall-effect, C-V and SIMS measurements were used to analyze the electrical properties, and both metal-organic MBE (MOMBE) growth and ion implantation studies showed the formation of hydrogen-complexes passivating shallow donor and acceptor states in GaN, InN, InAlN, and InGaN. Carbon incorporation in MOMBE growth of GaN was shown to produce p-type material. Since Al is expected to be highly reactive with impurities such as H and C, from the above considerations it would be disadvantageous to perform an n-type doping study of high Al content material using a growth system involving carbon and/or hydrogen containing sources or contamination

It would be advantageous to have a carbon and hydrogen-free system for doping studies of $Al_xGa_{1-x}N$ In the present research we employed a Varian Gen II MBE system equipped with cryopumps and ion pumps which are free of carbon contamination (oil-free pumps) and hydrogen- and carbon-free source materials (Ga, Al, Si, and N_2 gas)

Theoretical studies which attempt to explain the doping difficulties associated with AlGaN have been reported Stumm and Drabold[28] performed molecular dynamic, 96-atom simulations using wurtzite and zinc-blende AlN cells In their study substitutional incorporation of Si into the AlN matrix was considered and mid-gap defect states related to the Si-dopant were expected due to the large lattice relaxations around the Si atom. However, Stampfl and Van de Walle[29] performed first-principles calculations for the relevant native defects and dopant impurities in the $Al_xGa_{1-x}N$ system and these authors concluded that silicon was not expected to undergo a DX-type lattice relaxation and was expected to be a shallow donor as it is in GaN Wetzel *et al.*[30] through pressure studies on GaN have suggested that oxygen will exhibit DX type lattice relaxation in $Al_xGa_{1-x}N$ ($x > 0.4$) while silicon will remain a good hydrogenic donor for ($x > 0.56$)

Theoretical studies involving equilibrium calculations[29,31] on native point defects in AlN have predicted significant compensation effects for n- and p-type AlN by the formation of charged native defects In these studies, the formation energy of the triply-negatively charged aluminum vacancy (V_{Al}^{3-}) will become extremely small when the Fermi level is near the conduction band Therefore, when AlN is doped n-type, this charged vacancy will be formed to compensate the free electrons and the Fermi level will decrease until the material becomes insulating. Consequently, it would appear that in order to produce conducting *n*-type AlN, the formation of Al charged vacancies needs to somehow be restricted.

The work described in this dissertation was motivated by the need to develop methods of producing low resistivity *n*-type AlN and high Al-content AlGaN, aided by an understanding of the mechanisms that have prevented such an achievement thus far. In order to achieve this main goal, the present work had the following objectives. The first objective was to develop suitable *ex vacuo* and *in situ* substrate surface preparation procedures for epitaxial nitride growth. The second objective was to determine the growth conditions necessary to obtain low-temperature molecular beam epitaxy (MBE) growth of undoped AlN and AlGaN epilayers. The third objective was to develop ways to obtain conducting intentionally doped AlN. And the final objective was to understand how it is possible to produce such material.

Dissertation Outline

This dissertation is divided into six chapters. Chapter 1 includes a background review concerning epitaxial growth of high Al content AlGaN and the doping of such material.

Chapter 2 describes the growth and analytical techniques employed in this work and related system calibration results.

Chapter 3 presents a description of the sapphire crystal substrates used in this work and the development of suitable *ex vacuo* and *in situ* surface preparation techniques for MBE nitride growth.

Chapter 4 presents the sapphire surface nitridation, buffer layer and epilayer growth results and discussions.

Chapter 5 presents the Si-doping of AlN results obtained under various MBE growth conditions. A non-equilibrium theoretical model is presented to explain the experimental results.

Finally, Chapter 6 summarizes the conclusions drawn from this investigation.

CHAPTER 2
MBE GROWTH SYSTEM AND CHARACTERIZATION TECHNIQUES

Introduction

The samples in this work were grown by molecular beam epitaxy employing an rf plasma discharge, nitrogen free-radical source. The samples were analyzed using several analytical techniques, namely, atomic force microscopy (AFM), Hall-effect measurement, secondary ion mass spectrometry (SIMS), high-resolution X-ray diffraction (HRXRD), scanning electron microscopy (SEM), and electron microprobe.

MBE System

Overall System Configuration

The GaN, AlN, and AlGaN samples were grown using a Varian Gen II MBE system having three chambers: entry/exit chamber, buffer chamber (sample preparation chamber), and growth chamber. Each chamber has its own pumping capability, and an oil-free environment is ensured for all three chambers by using compressed air ventury pump and liquid nitrogen sorption pumps as roughing pumps and ion pumps and cryopumps as ultrahigh vacuum (UHV) pumps. Figure 2-1 shows a schematic of the Varian Gen II MBE system employed in this work. As illustrated in the figure, the MBE system consists of six components, namely, (1) sample preparation area, (2) entry/exit chamber, (3) buffer

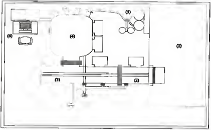

Figure 2-1 Schematic of the Varian Gen II MBE system used to grow III-V nitride epilayers

chamber (4) growth chamber, (5) gas source preparation area, and (6) computer control unit.

(1) Sample preparation area

The sample preparation area is for preparing and mounting the sample to the sample holder prior to loading the mounted sample into the entry/exit chamber. This area consists of loading table and chemical handling table. The chemical handling table includes the storage area for acids and other solvent chemicals and deionized water processing system. A hot plate with magnetic stirrer is located in the middle of the table. A hood system is provided above the chemical handling table in order to vent the evaporated chemicals.

(2) Entry/exit chamber

The entry/exit chamber is for the loading and unloading of samples. The chamber wall contains bakeout lamps with a water cooling reservoir. One end of the chamber is connected to the sample preparation area with a Viton ring high vacuum sealed door. The chamber is pumped by a CT-100 cryopump manufactured by Helix technology corporation. Roughing lines for initial pumping are also connected to the entry/exit chamber and cryopump. The other end of the roughing line is connected to the roughing pumps, namely the ventury pump and the liquid nitrogen sorption pumps. A rail for the sample transfer trolley is located at the bottom center of the chamber.

(3) Buffer chamber

The buffer chamber, also called the sample preparation chamber, is basically an ultrahigh vacuum (~ 10^{-11} Torr) chamber where the grown and to-be grown samples are placed on a sample transfer trolley. The chamber contains two magnetic transfer arms, one long and one short. The long transfer arm is to load samples into the growth chamber while the short is used during outgassing of the samples before loading them into the growth chamber. Sample outgassing is performed on the heating stage located on the other side of the short transfer arm.

(4) Growth chamber

The growth chamber used in this work (Figure 2-2) consists of several components: source flange, sample stage, RHEED system, and residual gas analyzer.

The source flange has a total of eight ports for the source materials. Four of the ports are downward looking and the remaining four ports are upward looking. Downward looking ports are for the sources which sublimate during growth, such as silicon, and beryllium. Upward looking ports can be used for all MBE source materials, however, they are used mostly for elements that evaporate from a liquid state, such as aluminum, gallium, and indium. Gas sources such as nitrogen can be place in any position. For this work, the nitrogen source was located on one of the downward looking ports.

The sample stage is composed of a substrate holder mechanism and a pressure measuring gauge, mounted back-to-back. The substrate holder mechanism includes a continuous azimuthal rotation (CAR) assembly. The CAR assembly is capable of handling up to 3-inch diameter wafers using a substrate mounting block, and it can be rotated 360°

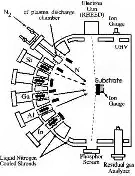

Figure 2-2 Schematic of MBE system used to grow Si-doped AlGaN

The two most-used sample stage positions are the transfer position and the growth position, which are positioned 180° apart. On the side of the sample stage opposite the substrate holder is an ion gauge that is used for measuring the pressure of the source material beam fluxes. This configuration is to measure the beam flux while the substrate is facing the opposite side and, therefore protection from the source beam fluxes. The substrate holder contains a tantalum heating filament, which heats the substrate mounting block by radiation A W-Re thermocouple is located at the center of the back side of the mounting block.

The growth chamber includes a RHEED system, which is capable of monitoring the evolution of the sample surface conditions during growth. A high-energy electron beam (8 8 keV) impinges on the sample surface at a grazing angle (~ 3°) and the resulting diffracted electrons excite a phosphor screen, creating a diffraction pattern.

In order to examine the gas species existing in the growth chamber, the growth chamber is equipped with a residual gas analyzer Under normal operating condition, no peak related to oxygen or carbon was detected by the gas analyzer

(5) Gas source preparation area

The gas source preparation area is designed to prepare the gas source before gas is introduced into the system. The source cylinders are stored in this area as well as the pumping system to purify the gas sources. A liquid nitrogen sorption pump was used to purge the gas line

(6) Computer control unit

The MBE modular Gen II system provides computer control of several components

- heating, cooling and shuttering of the eight molecular beam sources.
- heating, cooling, positioning and rotation of the substrate.
- heating and cooling of the entry/exit and buffer chambers

In order to control these tasks the computer hardware consists of the following components.

- DEC MICRO/PDP-11/73 process controller with 512 Kbyte random access memory (RAM)
- dual DSDD 5 1/4" floppy disk drives and a 10 Mbyte hard disk drive
- control console with interface to the MBE system.
- screen CRT terminal and multifunction keyboard.

The automation system uses the RSX-11M+ (DEC) operating system. The MBE automation software, version 7.0, enables the grower to consistently produce highly uniform epitaxial growth.

Effusion Cells for Al, Ga, and Si

An effusion cell is an evaporation source for use in ultra-high vacuum environments, having the following features:

1. Crucible, usually made from pyrolytic boron nitride (PBN), open on one end
2. Resistively heated filament

3. Thermocouple for monitoring and regulating temperature
4. Heat shielding to increase the efficiency of the cell and/or to protect the filament

Solid or liquid source material is placed in a crucible and is heated by passing current through the filament. The thermocouple data is fed into a closed loop control circuit for precise control of the temperature and, therefore, the evaporation rate. Each cell is equipped with a shutter that is controlled by pneumatic power. The shutter is not required to be vacuum tight, since the source beam is quite directional and the growth chamber walls are maintained at low temperature by circulating coolant (liquid nitrogen or chilled water). When the cell is at a stable temperature and the shutter is open, a beam flux from the source material exits the cell in the direction of the CAR assembly. The beam flux impinging on the substrate is measured in pressure units (Torr) by an ion gauge placed at the opposite side of substrate heater. In the transfer position, in which the ion gauge faces the effusion cells, the desired beam flux from each cell can be monitored.

Three different sizes of effusion cells were employed in this research: a 60cc cell for Ga, a 40cc cell for Al, and a 16cc cell for Si. The crucibles for all the cells are made of pyrolitic boron nitride (PBN), which does not react with these materials.

At operating temperatures, the Ga and Al source materials are in the liquid phase while the Si source material is in the solid state. Aluminum, however, wets the PBN crucible at high temperatures (~ 1000°C), while gallium and silicon do not. In addition, aluminum undergoes a large volume change during the liquid-solid phase transformation. Therefore, the aluminum cell should be handled with care during the heating and cooling stages, otherwise the crucible develops cracks, leading eventually to failure of the cell. Two safety cautions were employed to prevent crack development in Al crucible.

First, very slow cooling and heating rates were employed (less than 0.5°C per minute) for the cell temperature range of 550°C - 820°C (Al melting temperature = 660.4°C).

Second, an emergency power supply system was installed to protect the Al cell in the event of an electrical power failure, since, as a matter of routine, the Al is in the liquid state (at 820°C) even when the cell is idle. This emergency power circuitry is based on a design by Unger *et al.*,[32] and employs four 12V batteries. Relays provide automatic switching from the commercial electrical power source to the backup power source in the event of power failure. When the backup power system is in use, it will supply energy at a decreasing rate to allow slow cooling of the Al cell as the battery discharges. Several power resistors are connected to the battery in order to tune the slow cooling temperature range to that of the Al solidifying temperature range. After several experimental runs, a safe Al cell cooling curve was obtained during operation of emergency power system (Figure 2-3).

The gallium and aluminum effusion cells were tested at various temperatures in order to determine the flux/cell temperature relationship. The pressures of the Ga and Al incident beams were measured by the beam flux ion gauge (described above) at various cell temperatures. The evaporation phenomenon follows an Arrehnius equation.

$$P = A_0 \exp[-(E_{evp}/kT)]$$

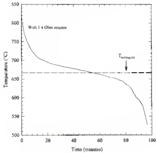

Figure 2-3 Al effusion cell emergency power supply cooling curve.

where P is the Ga or Al beam flux pressure. A_0 is a constant, E_{eva} is the Ga or Al evaporation energy, k is the Boltzmann constant and T is the absolute temperature. If we plot ln (P) versus 1/T, a linear relationship will appear and the slope of the line will be equal to E_{eva}/k. The evaporation energies of Ga and Al can be estimated from this graph. The results are plotted in Figure 2-4 for the Ga cell, and in Figure 2-5 for the Al cell.

Nitrogen Source

To generate nitrogen free radicals, an rf plasma discharge source manufactured by Oxford Applied Research (OAR), Oxfordshire, England, was used. A similar source was successfully used by Park[33] as a p-type dopant source during MBE growth of ZnSe and by others[34,35,36] for the MBE growth of GaN. Figure 2-6 shows the schematic of the nitrogen source. The source is mounted on the MBE growth chamber, via a 4.5" OD conflat flange, replacing a standard effusion cell. A high-precision UHV leak valve was used to introduce the nitrogen gas into the PBN discharge chamber.

The source of nitrogen was a cylinder of ultrapure nitrogen gas. Before introducing nitrogen gas into the chamber, the gas line was evacuated and backfilled several times using the ultrapure nitrogen to ensure the purity of gas that goes into the system.

Inductively-coupled rf energy at 13.56 MHz was used to generate the plasma by creating an electrical discharge with the presence of the nitrogen gas. To dissipate the heat generated during operation, both the discharge chamber and rf matching unit were water cooled. At the end of the discharge chamber, a PBN beam exit plate with 37 x 0.3mm diameter holes exists to release the nitrogen species to the growth chamber.

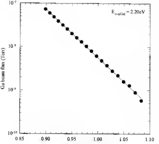

Figure 2-4 Ga effusion cell beam pressure vs. temperature profile

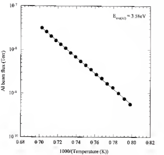

Figure 2-5 Al effusion cell beam pressure vs. temperature profile

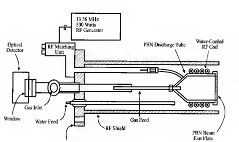

Figure 2-6 Schematic of rf plasma discharge source used to generate nitrogen free radicals (N)

A silicon photodiode was attached to the back-side window of the nitrogen source in order to measure the integrated plasma intensity. To examine the nitrogen species in the plasma, optical emission spectroscopy analysis was performed. Figure 2-7 illustrates the apparatus used. The emitted light from the plasma is focused into the spectrometer and dispersed by a 150 grooves/mm diffraction grating and finally detected by an array of 760 diodes placed linearly corresponding to the wavelengths of the dispersed optical signals. As a result, an emission spectrum (Figure 2-8) similar to that reported early by Park[23] was obtained. Over the emission wavelength range of 500 - 850 nm, five emission bands were observed resulting from the recombination of ground state nitrogen atoms (the so-called 1st positive system of nitrogen) and the direct relaxation of atomic nitrogen, both of which indicate the presence of nitrogen atoms in the plasma. There were no emission peaks related to the presence of nitrogen ionic species, which are expected to be seen in the range of 300 - 500 nm. The nitrogen plasma source conditions used in this work were a 250W rf forward power and a 1×10^{-5} Torr nitrogen beam flux, where only the emission peaks related to atomic nitrogen were present.

Substrate Temperature Calibration

The sample stage in the growth chamber is equipped with a W/Rh thermocouple located on the backside of substrate. However, the thermocouple is not physically attached to the substrate, and sapphire is also a poor heat conductor. Therefore, the thermocouple reading is expected to be quite different from the actual surface temperature of the substrate. In order to obtain a relationship between monitored temperature (thermocouple reading) and the actual

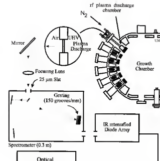

Figure 2-7 Schematic of optical emission spectroscopy apparatus used to characterize nitrogen plasma generated by rf discharge source

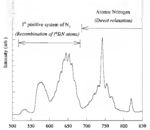

Figure 2-8 Molecular emission spectrum of nitrogen plasma generated from a 250 W, 13.56 MHz, rf plasma discharge with a nitrogen background pressure of 1 x 10^{-5} Torr.

temperature at the substrate surface, high vacuum temperature indicators were employed. Omega Temperature Indicating Liquids (OTIL) were chosen as the indicators since they have a time response to temperature changes on the order of milliseconds and an accuracy of ± 1% of the temperature reading. By applying a small amount of OTIL on a test sapphire surface which was mounted on a Mo block, it was easy to pinpoint at which monitored temperature the OTIL turned glossy from opaque, an irreversible change, indicating that the substrate had reached a particular temperature. Four OTILs with different temperature (621, 677, 732 and 804°C) were tested in this fashion, and the results are plotted in Figure 2-9. Uniformity of surface temperature was also tested using each OTIL at five different locations on the sapphire surface (the four corners and at the center). The change in appearance occurred at nearly the same time at all locations, indicating that the substrate surface temperature is uniform over a wide area.

Characterization Techniques

Atomic Force Microscope (AFM)

In order to study the surface roughness changes occurring during substrate preparation and epilayer growth procedures, AFM was employed in this work. The AFM system used in this work was a Nano Scope III Scanning Probe Microscope manufactured by Digital Instruments.

The AFM system can measure the force between the sample surface and a very sharp probe tip mounted on a cantilever beam having a spring constant of about 0.1 - 1.0 N/m, which is more than an order of magnitude lower than the typical spring constant

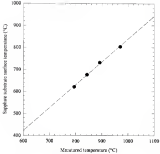

Figure 2.9 Plot of sapphire substrate surface temperature vs. monitored temperature obtained using Omega Temperature Indicating Liquids (OTIL)

between two atoms. The sample is placed on a scanner, the motion of which is controlled by piezoelectric tubes. If the force is determined as a function of the sample's position, then the surface topography can be obtained [37,38]. Both conducting and insulating materials can be analyzed without sample preparation.

The contact mode (using a silicon nitride tip) having a depth resolution of ~ 0.1 nm and a spatial resolution of a few nanometers was chosen for the analysis. A premeasured, smooth (RMS ~ 0.2nm) GaAs (001) sample was used as a reference sample to ensure the consistency of the system and the tips used in each measurement. Three areas having dimensions, 5μm x 5μm were selected randomly on each sample and the roughness results were averaged.

Hall-effect Measurements

A computer-controlled, custom-made Hall-effect measurement system was used to determine the electrical properties of variously prepared GaN, AlGaN and AlN epilayers. The Van der Pauw method[39] was employed to determine both the Hall coefficient and the resistivity of the films. Indium (99.95% purity) was used as a contact material and was applied by simply pressing a dot of indium onto the surface of the sample. Various magnetic field strengths (2 - 9 kGauss) were used and compared. A magnetic field strength of 9 kGauss was used since it gave the smallest error in the Hall coefficient and resistivity values.

Secondary Ion Mass Spectrometry (SIMS)

SIMS was used to compare the Si concentration in the variously prepared AlN epilayers. Cesium primary ions (Cs^+) with 5.0 kV energy were used to generate secondary ions which are detected by a quadrapole mass analyzer. A mass scan was made in order to determine the secondary ion species to be detected for the depth profile. Detecting Si in nitride materials can be tricky due to mass interference by $^{28}N_2$ and $^{28}CO^+$ with the $^{28}Si^-$ peak. In order to avoid this, one of the isotope peaks of Si, ^{29}Si was used to determine the Si concentration. The correct magnitude of the $^{28}Si^-$ signal was then estimated from the isotope ratio of 92.2/4.7 ($\%^{28}Si$ / $\%^{29}Si$). $^{41}AlN^-$ and $^{83}GaN^-$ were selected for the depth profile after the mass scan.

Additional scans were made for each sample by sputtering down to the first interface (AlN:Si / GaN interface). The sputtering rate was then determined from the scanning time and the depth measured by a mechanical profiler.

High Resolution X-ray Diffraction (HRXRD)

High resolution x-ray diffraction (HRXRD) was used to analyze the crystal quality of the (0001) sapphire substrates. A Philips diffractometer, model HR1, equipped with a Bartels four-Ge crystal monochromator[60] was used for this analysis. The (110) germanium crystals are set for either the 220 or 440 reflections of the CuKα radiation (the acceleration voltage and current were 40kV and 40mA, respectively). The four-crystal monochromator produces a nearly monochromatic x-ray beam with a very low divergence and low wavelength spreading. Figure 2-10 illustrates the function of the monochromator

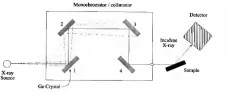

Figure 2-10 Schematic of five-crystal diffractometer

For sapphire crystal analysis, the monochromator setting was at the 220 reflection, and the 0006 reflection of the sapphire crystals was used for the rocking curve measurements. Three (0001) sapphire samples were randomly selected from various batches for the measurements, and the measured full width at half maximum (FWHM) values were averaged

Cross-sectional Scanning Electron Microscopy (SEM)

In order to determine the growth rate and film thickness uniformity, SEM images of epilayer cross-sections were used The samples were cleaved in half then mounted vertically, showing the flush cut cross-sectional area. Since the sapphire substrates used in this work were insulating, a Au-Pd coating was applied to the cleaved surfaces to prevent surface charging effects. Three images (one from the center and one from each edge) were taken from each sample to check the growth uniformity

Electron Microprobe

Electron microprobe, also called, electron probe X-ray microanalysis, (EPMA) is a spatially resolved, quantitative elemental analysis technique based on the generation of characteristic X-rays generated by a focused beam of energetic electrons[41,42] This technique was used in this work in order to verify the composition of epitaxial films grown at different growth temperatures but under fixed Al, Ga and N beam fluxes Insulating, undoped AlN and GaN standards were used to collect the characteristic X-ray signals of Al, Ga, and N, respectively The characteristic X-ray signal of each element in a AlGaN sample with unknown composition is then collected. The signals are compared with those of the standards for quantification. Wavelength spectrometry (WDS) was used to improve the detection limit down to the 0.01% range. However, the actual detection limit is expected to be higher due to the high absorption losses of the low-mass element (nitrogen) signal by the specimen and spectrometer components. All of the epilayer samples prepared for EPMA analysis were thick enough (greater than 1.0 μm) to avoid interference from the underlying layers (e.g., buffer layer and substrate).

CHAPTER 3
SUBSTRATE PREPARATION AND CHARACTERIZATION

Sapphire Substrates

The sapphire (Al_2O_3) substrates used in this work were purchased from Union Carbide Company. Table 3-1 lists the substrate specifications. The X-ray rocking curve full width at half maximum value was obtained by high-resolution XRD analysis.

Surface Cleaning

In the epitaxial growth process, the surface condition of the substrate plays a crucial roll, since the epilayer structure initially follows the surface arrangement of the substrate. The substrate surface needs to be free of contamination and unnecessary damage.

Such contamination or damage can be found in as-received sapphire substrates due to the handling procedures used by the manufacturers such as slicing, polishing, and packaging. In order to eliminate those defects and obtain an optimum surface condition for nitride growth, the following steps were developed.

Solvent Cleaning

A standard solvent cleaning method commonly used for Si and GaAs wafers was employed in this work to eliminate the organic contamination from the sapphire substrate

Crystal Size	11 x 10 mm
Crystal Orientation (on or off)	(0001) 0.3° off c-axis
Edges	Longer edges normal to a-axis
Crystal Thickness	0.4 mm
Carrier Type and Concentration	None (insulating)
Surface Finish	One side polished
Lattice Parameters	a = 4.758Å, c = 12.991Å
Thermal expansion coefficients	a-axis = 7.5 x 10^{-6} /K, c-axis = 8.5 x 10^{-6} /K
X ray Rocking Curve FWHM	13 arcsec (Figure 3.1)

Table 3-1 Specification of sapphire substrates used to grow GaN, AlN, AlGaN films.

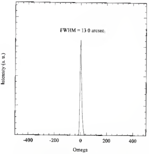

Figure 3-1 X-ray rocking curve of (0006) reflection obtained from a sapphire substrate crystal using HRXRD

surface The cleaning process began with three successive 5-minute boiling baths of trichloroethane, acetone, and methanol. After the methanol bath, the samples were rinsed in de-ionized water and then dried using nitrogen gas. After solvent cleaning, the surface morphology (roughness) of the solvent-cleaned sapphire was compared with the as-received sapphire surface by AFM (Figure 3-2) Similar surface roughnesses (RMS ~ 3Å) and images were recorded from both surfaces

Chemical Polishing (etching)

As reviewed in Chapter 1, a H_2SO_4 : H_3PO_4 (3:1) solution was chosen to chemically etch the sapphire surface A Thermex stirring-hot plate, model 310T was used to uniformly heat the H_2SO_4 : H_3PO_4 (3:1) solution. A thermometer held by an adjustable iron stand was placed in the middle of the etching solution to monitor the temperature A Teflon holder was used to immerse the samples in the solution. The solution was maintained at 160°C and stirred with a magnetic stirrer at medium speed during the etching process

Five samples etched for various lengths of time (10, 30, 60, 90, 120 minutes) and an as-received sample were compared by AFM analysis. Figure 3-3 plots the sample surface roughness against the etching time, and Figure 3-4 (a)-(f) shows the sample surface AFM images The figures indicate that the surface roughness is influenced by the etching time, initially decreasing and then increasing as the etching time increases. The minimum average surface roughness was obtained using a 90-minute etching time, as evidenced by a featureless surface Further etching (120 minutes) caused the surface

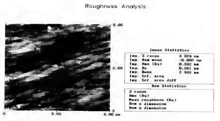

Image Statistics

Img. Z range	3.824 nm
Img. Raw mean	-0.006 nm
Img. Rms (Rq)	0.332 nm
Img. Ra	0.261 nm
Img. Rmax	3.309 nm
Img. Srf. area	
Img. Srf. area diff	

Box Statistics

Z range	
Rms (Rq)	
Mean roughness (Ra)	
Box x dimension	
Box y dimension	

(a)

Figure 3-2 AFM surface roughness analysis for (a) as-received (0001) sapphire surface
(b) solvent cleaned (0001) sapphire surface

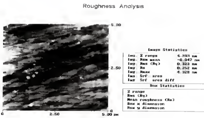

Image Statistics

```
Img. Z range           4.898 nm
Img. Raw mean         -0.047 nm
Img. Rms (Rq)          0.323 nm
Img. Ra                0.252 nm
Img. Rmax              4.328 nm
Img. Srf. area
Img. Srf. area diff
```

Box Statistics

```
Z range
Rms (Rq)
Mean roughness (Ra)
Box x dimension
Box y dimension
```

(b)

Figure 3-2 (continued)

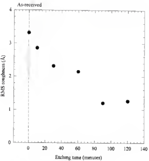

Figure 3-3 AFM RMS roughness of sapphire surface versus etching time in a mixture of 3:1 (H_2SO_4:H_3PO_4) solution at 160°C

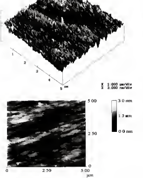

Figure 3-4 (a) AFM image of as-received c-plane (0001) sapphire surface

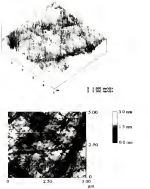

Figure 3-4 (b) AFM image of 10 minute etched c-plane (0001) sapphire surface

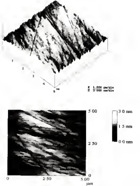

Figure 3-4 (c) AFM image of 30 minute etched c-plane (0001) sapphire surface

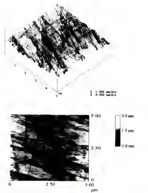

Figure 3-4 (d) AFM image of 60 minute etched c-plane (0001) sapphire surface

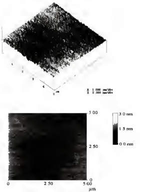

Figure 3-4 (e) AFM image of 90 minute etched c-plane (0001) sapphire surface

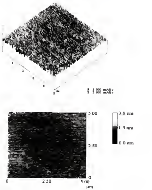

Figure 3-4 (f) AFM image of 120 minute etched c-plane (0001) sapphire surface roughness to increase slightly. It is believed that the driving force for the initial stage etching is to remove the polishing damage and further etching will lead to a selective etching related to the preferred etching directions in the crystal. Based on these results, a chemical etching time of 90 minutes was used to prepare the sapphire substrates for the epitaxially grown samples produced in this study.

In situ Thermal Cleaning

The chemically etched sapphire substrates were first loaded into the entry/exit chamber. After pumping the chamber until the pressure reached the ~10^{-8} Torr range, a bake-out was performed at 150°C for 1 hour. The samples were then moved into the buffer chamber where another bake-out was performed at 400°C for 20 minutes in the buffer chamber heating station. The purpose of the bake-outs was to desorb the absorbed or adsorbed water vapors from the freshly loaded trolley assembly containing the sapphire substrates and their mounts.

After the buffer chamber bake-out, the sapphire substrate were transferred to the growth chamber where they were thermally cleaned. The purpose of this thermal cleaning is to provide a sapphire surface ready to be reacted with the incoming nitrogen for surface nitridation. As discussed in Chapter 1, the best way to prepare such a surface is to form an Al-terminated surface preferably a ($\sqrt{3} \times \sqrt{3}$) 30° rotated arrangement. From early surface studies,[17-19] it is believed that a ($\sqrt{3} \times \sqrt{3}$) 30° rotated Al terminated arrangement might be achieved at surface temperatures above 900°C. However no such surface reconstruction was observed up to the maximum allowable surface temperature (940°C)

Figure 3-5 illustrate the RHEED patterns recorded in the $[11\bar{2}0]$ azimuth before and after thermal cleaning. Fairly diffuse patterns were recorded from the sapphire surface prior to the thermal cleaning, indicating a poorly ordered surface structure. As the surface temperature increased above 800°C, the pattern become clearer, showing streaky lines. Once the temperature reached near 900°C, no significant change in the RHEED pattern was observed and the pattern remained (1x1) up to the maximum allowable temperature (~940°C).

In order to study the impact of this thermal cleaning stage, five samples were thermally cleaned using various times (no cleaning, 10, 30, 60, and 120 minutes) at 940°C and were compared. The RHEED pattern remained streaky (1x1) and did not change in intensity or sharpness up to 120 minutes of thermal cleaning. However, the impact of the thermal cleaning time at 940°C appeared during subsequent surface nitridation. Only the samples thermally cleaned for more than 60 minutes showed completely nitrided RHEED patterns (patterns of AlN) after one hour exposure at a specific nitridation condition (see Chapter 4, Sapphire Nitridation). Samples that were thermally cleaned for less than 60 minutes exhibited a mixture of sapphire and AlN patterns after the nitridation.

Five samples that were cleaned thermally for various times (no cleaning, 10, 30, 60, and 120 minutes) at 940°C were compared by growing 0.4μm thick GaN epilayers under identical conditions after one hour of nitridation at 940°C.

The GaN epilayers were analyzed by AFM and Hall-effect measurements. The AFM roughness analysis results for the GaN epilayers suggest that thermal cleaning time has little or no effect on the epilayer surface morphology. However, Hall-effect

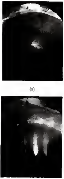

(a)

(b)

Figure 3-5 (0001) Sapphire surface RHEED patterns recorded (a) at RT, and (b) after *in situ* thermal cleaning at 940°C for 60 minutes measurements on the epilayers show the thermal cleaning time influence on the undoped GaN carrier concentration and mobility (Figure 3-7, 3-8). The resulting undoped GaN epilayers were all n-type. The figures clearly show a decrease in free electron concentration and an increase in electron mobility as the thermal cleaning time increases. It is also noticed that after a 60-minute thermal cleaning time no significant electron concentration or mobility change was observed. From the earlier RHEED observation on these samples during nitridation, the point at which complete nitridation occurred corresponded with the point where no further improvement in the undoped GaN electrical properties was observed. This result suggests that the degree of nitridation is important for the electrical properties of GaN epilayers, and it is closely related to the *in situ* thermal cleaning conditions. In this work, a thermal cleaning time of 60 minutes or more at 940°C was used in order to complete the nitridation process.

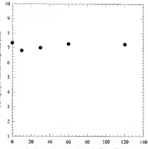

Figure 3-6 AFM data recorded from GaN epilayers grown on sapphire substrates that received various *in situ* thermal cleaning times at 940°C

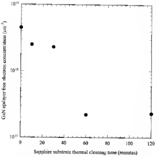

Figure 3-7 Free electron concentrations in GaN epilayers grown on sapphire substrates that received various *in situ* thermal cleaning times.

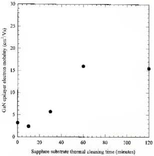

Figure 3-8 Free electron mobility in GaN epilayers grown on sapphire substrates that received various thermal cleaning times

CHAPTER 4
SAPPHIRE NITRIDATION AND III-V EPILAYER GROWTH

Sapphire Nitridation

The sapphire substrates prepared under the optimum conditions described in the previous chapter were exposed to the reactive nitrogen flux for nitridation. The nitridation process involves the formation of AlN on the sapphire surface. Five samples were prepared using various nitridation times (10, 30, 60, 120 180 minutes of N flux exposure) to study the nitridation development. Also, GaN epilayers were deposited under fixed growth conditions to study the influence of nitridation time on epilayer growth. The sapphire surface nitridation was performed at 940°C with an rf forward power of 250W and a nitrogen flux of $1\text{x}10^{-5}$ Torr. The integrated plasma intensity recorded by the silicon photodiode was ~90 meV under these conditions.

RHEED Analysis

A series of RHEED patterns recorded during the nitridation process is shown in Figure 4-1. The incident electrons had an energy of 8.85 keV. In these photographs, the two diffraction lines on either side of the center line in the patterns recorded in the $[11\bar{2}0]$ azimuth (30° away) disappear during the 120-minute nitridation process. Also, the spacing between the lines in the pattern recorded in the $[10\bar{1}0]$ azimuth (0° reference)

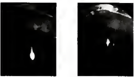

(a) 0° reference (sapphire)　　(b) 30° away (sapphire)

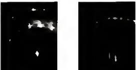

(c) 0° reference (10-minute nitridation)　　(d) 30° away (10-minute nitridation)

Figure 4-1 RHEED patterns recorded after various nitridation times (a), (c), (e), (g), (i), and (j) were recorded in [$10\bar{1}0$] and (b), (d), (f), (h), (j), and (k) were recorded in [$11\bar{2}0$]

(e) 0° reference (30-minute nitridation) (f) 30° away (30-minute nitridation)

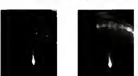

(g) 0° reference (60-minute nitridation) (h) 30° away (60-minute nitridation)

Figure 4-1 (continued)

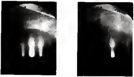

(i) 0° reference (120-minute nitridation) (j) 30° away (120-minute nitridation)

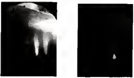

(k) 0° reference (180-minute nitridation) (l) 30° away (180-minute nitridation)

Figure 4-1 (continued)

increases over time. These changes can be analyzed to understand the transformation the sapphire surface is undergoing during nitridation.

Figure 4-2 shows a schematic of the RHEED diffraction patterns and their relationship to the actual crystal surface configuration. In the diffraction phenomenon, crystalline plane spacings perpendicular to the incident beam direction are inversely proportional to the diffracted line spacing. Therefore, one can determine the lattice structure of the surface by examining the RHEED diffraction line spacing. First, the RHEED pattern line spacings from thermally cleaned sapphire were compared. The line spacings were 7.7mm and 13.2mm for the RHEED patterns recorded in the $[11\bar{2}0]$ and $[10\bar{1}0]$ azimuth, respectively. As illustrated in Figure 4-2, the distance between planes of sapphire in the $[10\bar{1}0]$ direction is $a_0/2 = 2.379$Å and for the $[11\bar{2}0]$ direction it is $a_0\sqrt{3}/2 = 4.120$Å. If the line spacing of 13.2mm is from the $[10\bar{1}0]$ direction, the line spacing of the $[11\bar{2}0]$ direction can be calculated using the known plane spacing of sapphire in each direction.

$$\begin{aligned}\text{Line spacing at } [11\bar{2}0] &= 2.379\ (\text{Å}) \times (\text{Line spacing at (mm) } [10\bar{1}0] / 4.120\ (\text{Å}))\\ \text{(Sapphire)} \qquad &= 2.379 \times 13.2 / 4.120\\ &= 7.62\ (\text{mm})\end{aligned}$$

The calculated result (7.62mm) closely matches the line spacing value (7.7mm) observed from the $[11\bar{2}0]$ sapphire surface.

During nitridation, the RHEED pattern line spacing in the $[10\bar{1}0]$ azimuth of sapphire changes from 13.2mm initially to 13.0mm after a 10-minute nitridation and finally decreases to 11.8mm after a 30-minute nitridation. The spacing remains at 11.8mm for

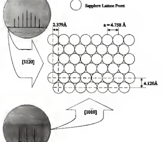

Figure 4-2 Illustration of sapphire RHEED patterns related to the actual surface arrangement

60- and 120-minute nitridations. The $[10\bar{1}0]$ sapphire line spacing was compared with the final line spacing of 11.8mm after a 30- or more minute nitridation time

$$\begin{array}{ll} \text{Planar distance} & = 13.2\ (\text{mm}) \times 2.379\ (\text{Å}) / 11.8\ (\text{mm}) \\ ([11\bar{2}0]\ \text{AlN}) & = 2.661\ (\text{Å}) \end{array}$$

This value closely matches the $[11\bar{2}0]$ direction planar distance of AlN,

$$\begin{array}{ll} \text{Planar distance} & = a_{\text{(AlN)}} \times \sin 60° = 3.1114\ (\text{Å}) \times \sqrt{3}/2 \\ ([11\bar{2}0]\ \text{AlN}) & = 2.694\ (\text{Å}) \end{array}$$

In order to verify the formation of AlN on the (0001) sapphire surface, the $[11\bar{2}0]$ sapphire azimuth RHEED pattern change was compared with the pattern after nitridation. As shown in Figure 4-1, every third line from the $[11\bar{2}0]$ sapphire pattern remains while the other lines gradually disappear over the time period of ~ 90 minutes. After the lines disappeared, no further pattern change was observed. The line spacing becomes 20.0mm which agrees well with the calculated line spacing for the $[10\bar{1}0]$ azimuth of AlN.

$$\begin{array}{ll} \text{Line spacing at } [10\bar{1}0] & = 2.694\ (\text{Å}) \times (\text{Line spacing at } [11\bar{2}0]\ (\text{mm}) / 1.556\ (\text{Å})) \\ (\text{AlN}) & = 2.694 \times 11.8 / 1.556 \\ & = 20.43\ (\text{mm}) \end{array}$$

From these results, the relationship between sapphire and the AlN formed during nitridation can be derived as $[11\bar{2}0]$ sapphire // $[10\bar{1}0]$ AlN and $[10\bar{1}0]$ sapphire // $[11\bar{2}0]$ AlN. This agrees with the earlier argument that suggested the formation of a 30° rotated AlN structure on sapphire during the nitridation process (see Chapter 1), since $[11\bar{2}0]$ is 30° rotated from $[10\bar{1}0]$ in a hexagonal structure.

A set of GaN epilayers was grown directly on substrates that were processed using various nitridation times. A 60-minute *in situ* thermal cleaning at 940°C, followed by nitridation times of ~0, 10, 30, 60, 120, 180 minutes were used for each sample prior to GaN growth. The RHEED pattern development was quite similar among all the samples, including the apparent initial transition from 3-D to 2-D planar growth.

AFM Analysis

Sapphire substrates prepared using the various nitridation times (0, 10, 30, 60, 120, 180 minutes) as well as GaN epilayers grown on such surfaces were examined by AFM. All samples were prepared by solvent cleaning, 90-minute chemical etching and 60-minute *in situ* thermal cleaning at 940°C prior to the nitridation and epilayer growth steps.

Figure 4-3 illustrates sapphire surface roughness data plotted against nitridation time obtained from the AFM measurements. As can be seen from the figure, the surface roughness increases abruptly initially and then decreases to a value close to the original sapphire surface roughness after 30 minutes of nitridation. Nitriding for times beyond 60 minutes appears to further roughen the surface. However, the surface roughness of GaN films grown on the variously nitrided sapphire substrates appears to be independent of nitridation time (Figure 4-4).

Hall-effect Measurements

All nitrided sapphire samples as well as the as-received sapphire substrates were insulating. However, the GaN epilayers grown directly on the substrates that were

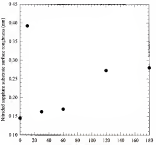

Figure 4-3 AFM data recorded from nitrided sapphire substrates that were nitrided for various times

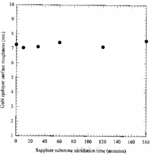

Figure 4-4 AFM data recorded from GaN epilayers grown on sapphire substrates that were nitrided for various times.

processed using various nitridation times were all conducting n-type. The dependences of the GaN epilayer carrier concentration and mobility on the sapphire substrate nitridation time are shown in Figure 4-5 and 4-6, respectively. The free electron concentration decreases and electron mobility increases as the nitridation time increases.

It is interesting to note that the electrical properties of GaN epilayers were sensitive to the substrate nitridation time even though there was no significant difference in the RHEED pattern development and AFM analysis. Along with the AFM results from the *in situ* thermal cleaning experiment (Figure 3-6), it has been clearly shown that the surface roughness of the GaN epilayers is independent of the initial stage of the growth, while the epilayer electrical properties can be improved by optimizing the initial preparation of the sapphire substrate surface. The earlier RHEED analysis suggests that only after a 60-minute nitridation treatment does the pattern become that of relaxed AlN, suggesting that the initial increase and decrease in roughness as the nitridation time increases up to 60 minutes is related to the nucleation and accommodation of the strained AlN structure on the sapphire surface. After a 60-minute nitridation treatment, the AlN seems to be relaxed by the formation of misfit defects. As a result, the surface roughness is expected to increase again as the nitridation time increases.

Epitaxial growth of the nitride structure (e.g. GaN) on a surface having incomplete nitridation might result in an increase in the kinetic barrier for the formation of the nitride. As a result, the formation of other defects such as nitrogen vacancies, known to be shallow donors in GaN, can be encouraged. Further nitridation (after 120 minutes) does not provided any significant change in the GaN electrical properties. It seems that the

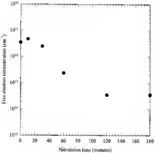

Figure 4-5 Free electron concentration versus nitridation time for GaN epilayers grown on nitrided sapphire surfaces.

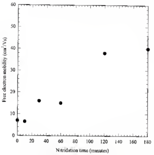

Figure 4-6 Free electron mobility versus nitridation time for GaN epilayers grown on nitrided sapphire surfaces

surface AlN formation on sapphire by the nitridation process is limited to only a few atomic layers either due to nitrogen diffusion limitations at the nitridation temperature or due to the difference in reactivities between the bulk and the surface atoms of such prepared sapphire. The sapphire thermal cleaning study discussed in Chapter 3 showed that complete nitridation could be achieved only after a sufficient thermal cleaning time. This observation strongly favors the latter reason that the reactivity difference between bulk and surface atoms limits the nitridation.

Based on these considerations, a nitridation time of 120 minutes was employed during substrate preparation for the epitaxial samples grown in this study, since a suitable AlN structure for nitride growth is expected to be formed using this nitridation time and no improvement is expected from further nitridation.

AlN Buffer Layer Growth

Epilayer deposition directly on such nitrided surfaces, however, is not desirable. Although the AlN structure formed by nitridation is assumed to be relaxed, the few atomic layers of AlN thus formed are not expected to accommodate all of the undesirable defects. A buffer layer, having the nitride structure, that can contain most of these defects is considered a desirable method to improve the epilayer quality.

Both AlN and GaN are considered as buffer layer candidate materials in the literature. However, AlN was chosen over GaN in this work as a buffer layer since insulating GaN epilayers could be grown on top of AlN buffers. A conducting buffer layer was not desirable for this study since Hall effect measurements were planned which require electrical isolation.

AlN buffer layers grown at high growth temperatures (higher than 800°C) were compared with layers grown at low temperatures (lower than 800°C). All of the AlN buffer layers studied in this work were insulating. However, GaN layers grown on the high-temperature AlN buffer layers were insulating, while GaN layers grown on the low-temperature AlN buffers were conducting (n-type, $>10^{17}$ cm^{-3}). Consequently, high-temperature AlN buffers were selected in this work.

RHEED Analysis

Figure 4-7 shows the RHEED pattern development for the AlN buffer layers grown under various conditions. An Al beam flux of 2.7×10^{-6} Torr and a 250W rf forward power for the nitrogen source were used for sample growth. Growing an AlN buffer layer at the low temperature of 750°C resulted in amorphous material (Figure 4-7(b)). The patterns recorded following annealing at 880°C, however, show a clear transition from amorphous to crystalline material (Figure 4-7(b)-(d)). The spotty RHEED pattern recorded at the end of an 18-minute annealing indicates poor morphology. Further annealing did not improve the RHEED pattern. In contrast, the RHEED patterns recorded during AlN buffer layer growth at 900°C indicated crystalline surfaces throughout (Figure 4-8). The nitrided substrate pattern initially became diffuse and dimmed a little (Figure 4-8 (b)), however, the line width and brightness recovered over a period of time (Figure 4-8 (c)-(d)). At the end of 20 minutes, a sharp streaky pattern was recorded, indicating that the growing surface was smooth. Throughout the growth at

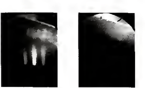

(a) Sapphire substrate (b) Initial deposition of AlN at 750°C

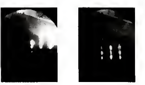

(c) After 10-minute anneal at 880°C (d) After an 18-minute anneal at 880°C

Figure 4-7 RHEED patterns recorded during the deposition at 750°C and the subsequent annealing at 880°C of an AlN buffer layer on sapphire. Note that the deposited layer was initially amorphous.

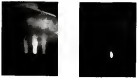

(a) Sapphire substrate

(b) After 1 minute of AlN growth

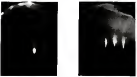

(c) After 10 minutes of AlN growth

(d) After 20 minutes of AlN growth

Figure 4-8 RHEED patterns recorded from an AlN buffer layer grown directly at 900°C Note that the AlN was crystalline throughout growth.

900°C, 2-D planar growth prevailed, as indicated by the observation of a streaky RHEED pattern during growth.

AFM Analysis

Figure 4-9 shows the results of AFM roughness analysis on the low- (750°C) and high- (900°C) temperature AlN buffer layers. The buffer layer thickness was expected to be the same (~300Å) for both cases, as indicated by growth rate experiments associated with thick AlN layers deposited using similar growth conditions. As expected from RHEED analysis, a much smoother surface was produced using the high AlN growth temperature.

Undoped AlGaN Epilayer Growth

First, AlN growth was attempted on high-temperature AlN buffers. RHEED analysis was used to monitor the surface structure change during each growth parameter change, namely III/V beam flux ratio, growth temperature and the presence of a second buffer (GaN).

Then, the optimized AlN growth conditions were used to grow high Al-content AlGaN. A fixed Ga flux of 7×10^{-7} Torr and a growth temperature range of 850 – 940°C were employed. The AlGaN epilayers were analyzed by electron microprobe to determine the epilayer compositions.

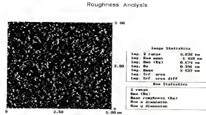

Image Statistics

Img. Z range 8.838 nm
Img. Raw mean 1.458 nm
Img. Rms (Rq) 0.674 nm
Img. Ra 0.391 nm
Img. Rmax 9.637 nm
Img. Srf. area
Img. Srf. area diff

Box Statistics

Z range
Rms (Rq)
Mean roughness (Ra)
Box x dimension
Box y dimension

(a)

Figure 4-9 AFM surface roughness analysis for (a) low temperature AlN buffer surface
(b) high temperature AlN buffer surface

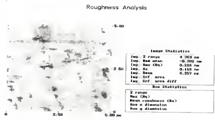

```
          Image Statistics
Img. Z range            4 363 nm
Img. Rms mean           -0.002 nm
Img. Rms (Rq)           0.228 nm
Img. Ra                 0.159 nm
Img. Rmax               4.357 nm
Img. Srf. area
Img. Srf. area diff
           Box Statistics
Z range
Rms (Rq)
Mean roughness (Ra)
Box x dimension
Box y dimension
```

(b)

Figure 4-9 (continued)

Undoped AlN Epilayer Growth

A series of AlN films was deposited at various substrate temperatures (820, 850, 880, and 940°C) under a fixed III/V flux ratio (2.7×10^{-2}) on high-temperature AlN buffer layers. RHEED analysis showed that planar epitaxial growth was obtained for samples grown at 880°C or higher. AlN layers grown below 880°C were not epitaxial, as evidenced by the appearance of an arc or ring pattern during growth. By decreasing the III/V ratio to 2.7×10^{-3}, epitaxial AlN growth was obtained for growth temperature as low as 850°C. Further decreasing the III/V ratio resulted in a spotty RHEED pattern. The growth rate decreased from 0.3μm/hr to 0.1μm/hr as the III/V ratio decreased. An increase in surface migration associated with the decrease in growth rate is thought to be the reason why the epitaxial growth temperature could be lowered by reducing the III/V ratio.

Another series of AlN films was deposited at various substrate temperatures (820, 850, 880, and 940°C) this time on insulating GaN (buffer) layers grown on high temperature AlN buffers. The GaN buffer layer was grown at 750°C, using a Ga flux of 7.0×10^{-8} Torr, a 250W rf forward power and a nitrogen background pressure of 1×10^{-5} Torr. The GaN buffer layer thickness was 0.1 μm. Epitaxial AlN was achieved at 850°C or higher.

All of the undoped AlN films prepared in this study were insulating regardless of the growth conditions used. Therefore, it was difficult to deduce the influence of the GaN buffer layer from the properties of the AlN epilayer. The apparent difference between the AlN epilayers grown on a GaN buffer and those grown directly on a high-temperature AlN buffer was the initial sharpness of the RHEED pattern during epilayer growth. Figure 4-10 shows the initial and the final RHEED patterns recorded from AlN epilayers grown on buffer layers deposited under different conditions. The diffraction lines recorded during initial AlN epilayer growth on a GaN buffer layer were sharper than those recorded from AlN grown directly on a high temperature AlN buffer layer. However, after four hours of AlN growth, similar patterns were recorded from both layers. The sharpness of the RHEED pattern streaks can be correlated to the crystal quality of the growing surface. Therefore, the presence of a GaN buffer layer is believed to improve the initial quality of the AlN epilayers.

Undoped AlGaN Epilayer Growth

Growth conditions for the previously described AlN epilayer growth (with GaN buffer layers) were used to grow AlGaN epilayers. A Ga flux (7×10^{-8} Torr) was simply added during the growth, and three different growth temperatures (850, 880, 940°C) were employed. No observable difference in the RHEED pattern was noticed during the growth of these films. The films were analyzed by electron microprobe to determine their composition. The samples grown at 850 and 880°C had ternary compositions of $Al_{0.75}Ga_{0.25}N$, and $Al_{0.83}Ga_{0.17}N$, respectively. The sample grown at 940°C was determined to be AlN. Hall-effect measurements indicated that all of the samples were insulating.

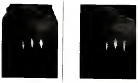

(a) after 3 minutes of growth

(b) after 4 hours of growth

(c) after 3 minutes of growth

(d) after 4 hours of growth

Figure 4-10 RHEED patterns recorded during AlN epilayer growth (a) and (b) without a GaN buffer layer, (c) and (d) with a GaN buffer layer

CHAPTER 5
Si-DOPING OF HIGH Al-CONTENT AlGaN

Si-doped samples were systematically grown under various conditions to determine the influence of each growth parameter on the doping of AlGaN with Si. In all cases a Si effusion cell temperature of 1280°C was used, which results in a Si doping concentration of ~10^{19} cm^{-3} in GaN grown using a similar growth rate (~ 0.1 μm/hr). The influences of three crucial parameters, namely, growth temperature, GaN buffer layer, and the addition of a Ga flux, were studied. A non-equilibrium model based on thermodynamics and kinetics was developed to explain the experimental observations.

Experimental Results

Influence of Growth Temperature

Si-doped AlN epilayers were deposited using various growth temperatures. Figure 5-1 shows a plot of the resistivity values obtained from Hall-effect measurements, as a function of growth temperature. Si-doping work at growth temperatures below 850°C was excluded since, as discussed in the previous chapter, the RHEED pattern gradually disappears, indicating that epitaxial growth of AlN is not possible at such low temperatures.

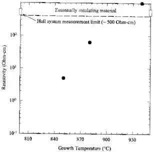

Figure 5-1 Resistivity data obtained from Si-doped AlN films grown at various substrate temperatures.

A strong temperature dependence of resistivity was observed for a fixed Si flux. At growth temperatures above 900°C, the AlN films were insulating ($\rho > 500\ \Omega$cm) while at growth temperatures below 900°C, the AlN films were conducting ($\rho < 100\ \Omega$cm). In the absence of a Si flux, all of the AlN films were insulating regardless of growth temperature.

For the conducting AlN films, carrier type, concentration, and mobility values were difficult to resolve due to large fluctuation in Hall voltage values under applied magnetic fields (5~9 kGauss). Despite the fluctuating Hall voltage, the sign of Hall voltage was mainly negative, implying n-type conduction.

In order to examine the amount of Si incorporation in the AlN films, the three samples whose resistivity values are plotted in Figure 5-1 were analyzed by SIMS. The data (Figure 5-2, 5-3, and 5-4) suggest that the Si concentrations are similar in all three samples and, hence, the resistivity variation with growth temperature is due to something other than Si impurity concentration.

Influence of GaN Buffer Layer

A set of Si-doped AlN samples was grown this time without GaN buffer layers but otherwise using the same growth conditions as above. As can be seen from Figure 5-5, all of the AlN films grown without a GaN buffer layer were insulating regardless of growth temperature. The data from the previous set of samples is also shown in Figure 5-5 for comparison purposes. A difference in the RHEED pattern was observed for the epilayer growth at 850°C. At a growth temperature of 850°C, a transition in the RHEED pattern

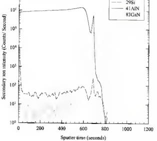

Figure 5-2 SIMS depth profile of a Si-doped AlN film grown at 850°C

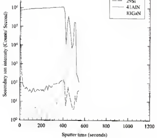

Figure 5-3 SIMS depth profile of a Si-doped AlN film grown at 880°C

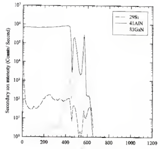

Figure 5-4 SIMS depth profile of a Si-doped AlN film grown at 940°C.

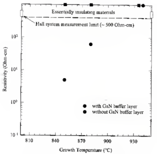

Figure 5-5 Resistivity data obtained from Si-doped AlN films grown at various substrate temperatures with and without a GaN buffer layer

from streaky lines to elongated spots was observed (Figure 5-6) during the growth of Si-doped AlN without a GaN buffer layer, while the AlN grown on a GaN buffer exhibited a streaky pattern throughout. This streaky to spotty RHEED pattern transformation is an indication of a 2D-3D growth front change. Indeed, a rougher surface was indicated from AFM roughness analysis (Figure 5-7), which agrees with the RHEED observations.

Influence of the Presence of a Ga Flux

The influence of the presence of a Ga flux during growth was studied by adding a flux of Ga during Si-doping of AlN. The resistivity data obtained from the samples are shown in Figure 5-8. The figure shows that by introducing a Ga flux while doping, the resistivity decreased about two orders of magnitude regardless of growth temperature. In order to find out how much of the Ga was actually incorporated, electron microprobe analysis was performed. The analysis indicated that the samples grown at 850 and 880°C had compositions of $Al_{0.75}Ga_{0.25}N$ and $Al_{0.93}Ga_{0.07}N$, respectively, while the Ga concentration was below the detection level (~ 1%) for the sample grown at 940°C.

SIMS analysis was performed on the Si-doped AlN films grown at 940°C, one with a Ga flux present during growth, the other without a Ga flux present. An interesting observation was that in the sample grown with a Ga flux, although only a trace amount of Ga was actually incorporated, the ^{29}Si signal increased almost an order of magnitude above that of the sample grown without a Ga flux. The Si concentration also appears to be much more uniform as a function of film thickness in the case of the Si-doped AlN film grown in the presence of a Ga flux.

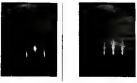

(a) after 3-minute growth (b) after 4-hour growth

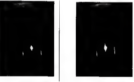

(c) after 3-minute growth (d) after 4-hour growth

Figure 5-6 RHEED patterns recorded at 850°C during Si-doped AlN epilayer growth (a) and (b) without a GaN buffer layer; (c) and (d) with a GaN buffer layer

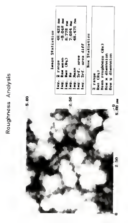

```
Image Statistics
Img. Z range            48.428 nm
Img. Raw mean           -0.048 nm
Img. Rms (Rq)            8.778 nm
Img. Ra                  7.084 nm
Img. Rmax               48.475 nm
Img. Srf. area
Img. Srf. area diff
        Box Statistics
Z range
Rms (Rq)
Mean roughness (Ra)
Box x dimension
Box y dimension
```

(a)

Figure 5.7 AFM surface roughness analysis for Si doped AlN epilayers grown (a) without a GaN buffer layer, (b) with a GaN buffer layer

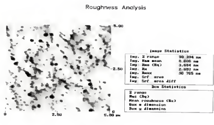

Roughness Analysis

Image Statistics

Img. Z range 30.394 nm
Img. Raw mean 8.006 nm
Img. Rms (Rq) 3.684 nm
Img. Ra 2.803 nm
Img. Rmax 30.765 nm
Img. Srf. area
Img. Srf. area diff

Box Statistics

Z range
Rms (Rq)
Mean roughness (Ra)
Box x dimension
Box y dimension

(b)

Figure 5.7 (continued)

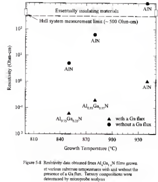

Figure 5-8 Resistivity data obtained from $Al_xGa_{1-x}N$ films grown at various substrate temperatures with and without the presence of a Ga flux. Ternary compositions were determined by microprobe analysis

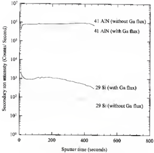

Figure 5-9 Si profiles obtained by SIMS analysis in Si-doped AlN films grown with and without the presence of a Ga flux at a substrate temperature of 940°C.

Theoretical Model

A theoretical model was developed in order to explain the experimental results. The model includes thermodynamic and kinetic considerations. The possibility of n-type, Si-doping of AlN is discussed for the case of thermodynamic equilibrium. Specific non-equilibrium growth conditions were then evaluated followed by kinetic considerations of Si-doping with and without the presence of a Ga flux. Finally the model was tested by applying it to the experimental situations.

Thermodynamic Consideration

Assuming that there are a very small number of defects (vacancies) compared to the number of constituent elements. The free energy of the system is

$$G = H - TS \qquad \text{------(1)}$$

where G is Gibbs free energy, H is the enthalpy, T is the absolute temperature, and S is the entropy. The free energy change of the lattice due to the presence of n number of vacancies is

$$\Delta G = nH_v^f - T(S + nS_v^f) \qquad \text{------(2)}$$

where H_v^f is the formation enthalpy of a vacancy, S_v^f is the vibrational entropy, and S is the configurational entropy of mixing between vacancies and atoms in a lattice. The Boltzmann expression of entropy

$$S = k \ln W \qquad \text{------(3)}$$

where k is the Boltzmann constant, and W is the number of ways for arranging the defects(vacancies) in a crystal. Assuming there are n vacancies in a crystal of N lattice sites, we obtain

$$W = \frac{N(N-1)---(N-n+1)}{n!}$$

$$= \frac{N!}{(N-n)!n!} \qquad \text{------}(4)$$

applying equation (4) to (3)

$$S = k \ln \frac{N!}{(N-n)!n!} \qquad \text{------}(5)$$

Using the Stirling's approximation ($\ln x! \approx x \ln x$, when x is large)

$$S = k\,(N \ln N - (N-n) \ln (N-n) - n \ln n] \qquad \text{------}(6)$$

From equation (2) and (6)

$$\Delta G = nH_v^f - T(nS_v^f + k[N \ln N - (N-n) \ln (N-n) - n \ln n]) \qquad \text{------}(7)$$

Under thermodynamic equilibrium,

$$\frac{\partial \Delta G}{\partial n} = 0 \qquad \text{------}(8)$$

From equation (7) and (8) we have

$$\frac{\partial \Delta G}{\partial n} = H_v^f - TS_v^f - T[k \ln \frac{(N-n)}{n}] = 0$$

$$H_v^f - TS_v^f - kT \ln \frac{(N-n)}{n} = 0$$

rearranging gives,

$$\frac{n}{N-n} = \exp(\frac{S_v^f}{k}) \exp(-\frac{H_v^f}{kT}) \qquad \text{------}(9)$$

From the early assumption that N>>n

$$\frac{n}{N} = \exp(\frac{S_v^f}{k})\exp(-\frac{H_v^f}{kT})$$

$$n = N\exp(\frac{S_v^f}{k})\exp(-\frac{H_v^f}{kT}) \qquad \text{------}(10)$$

The formation energy of a vacancy is defined as

$$\Delta G_v^f = H_v^f - TS_v^f$$

$$n = N\exp(\frac{-\Delta G_v^f}{kT}) \qquad \text{------}(11)$$

The formation energy of a defect in a charged state q is

$$\Delta G_v^f(q) = E_{defect}^{tot}(q) - \sum_x n_x \mu_x + qE_F \qquad \text{——}(12)$$

Where $E_{defect}^{tot}(q)$ is the total energy of the defect, and n_x and μ_x are the number and chemical potential of atoms of species x, respectively. E_F is the Fermi energy, which is set to zero at the top of the valence band.

Stampfl and Van de Walle[28] and Mattila and Nieminen[31] have calculated $E_{defect}^{tot}(q)$ and the formation energy of various point defects in AlN. The results suggest that the V_{Al}^{3-} formation energy becomes extremely small when the Fermi energy is near the conduction band. Therefore, whenever the material is doped n-type, there will be a counter force (compensation) by the formation of these charged defects, which will pin the Fermi level near the midgap rendering the material insulating. This compensation is particular to the wide bandgap materials, since the qE_F term in equation (12) will dominate the defect formation energy. In the case of V_{Al}^{3-} the qE_F term dominates so much that when E_F is in the conduction band, the formation energy can be estimated as,

$$\Delta G_A^{3-} = a_0 \quad 3(E_F - E_C) \qquad \cdots\cdots (13)$$

$(E_F - E_C)$ values for n-type AlN with various free electron concentrations were calculated and the result are plotted in Figure 5-10. An electron effective mass of 0.33 was used (after Ref. 43), and the value for a_0 was determined from the formation energy at the conduction band[16] $(E_F = E_C)$. Figure 5-11 shows the resulting V_{Al}^{3-} formation energies at various Fermi energies.

The equilibrium concentration of V_{Al}^{3-} is then calculated from equation (11). The number of lattice sites (N) is calculated from the lattice parameters of AlN ($N = 4.786 \times 10^{22}$ cm^{-3}). The result is plotted as a function of temperatures in Figure 5-12. It is clear from the figure that no matter what free electron concentration exists, it will get compensated by the formation of V_{Al}^{3} and the resulting AlN will become insulating. Note that the V_{Al}^{3} concentrations in Figure 5-12 are imaginative numbers calculated from the formation energy.

Free carrier compensation is more of a dynamic process. Once the V_{Al}^{-3} concentration approaches the free electron concentration, the resulting compensation will drop the Fermi energy, which will prevent further formation of V_{Al}^{-3} due to the increased formation energy. Therefore, the V_{Al}^{-3} concentration cannot be larger than the free electron concentration of a material.

Figure 5-12 was obtained under thermodynamic equilibrium conditions (equation (8)). In real situations, however, thermodynamic equilibrium does not occur especially,

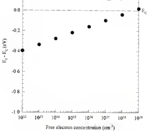

Figure 5-10 AlN Fermi energy versus free electron concentration.

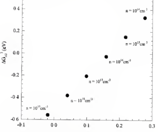

Figure 5.11 Calculated formation energy of V_{Al}^{3-} at various free electron concentrations

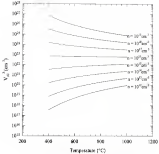

Figure 5-12 Equilibrium aluminum vacancy concentration versus temperature at various free electron concentrations in n-type AlN

when a non-equilibrium growth method such as MBE is employed. In order to understand the native defect formation under non-equilibrium situations, the following steps were made.

Under non equilibrium conditions

$$\frac{\partial \Delta G}{\partial n} \neq 0 \qquad \text{-------}(14)$$

Define α as a non-equilibrium factor

$$\frac{\partial \Delta G}{\partial n} = \alpha \qquad \text{-------}(14)$$

from equations (7) and (14)

$$\frac{\partial \Delta G}{\partial n} = H_v^f - TS_v^f - kT\ln\frac{(N-n)}{n} = \alpha \qquad \text{------}(15)$$

after rearranging the terms

$$n = N\exp(\frac{-\Delta G_v^f}{kT})\exp(\frac{\alpha}{kT}) \qquad \text{------}(16)$$

equation (16) can be written as

$$n = N\exp(\frac{-(\Delta G_v^f - \alpha)}{kT}) \qquad \text{------}(17)$$

The value α is defined in equation (14) as the free energy change of the system brought on by a change in the concentration of a specific type of defect. The change in α value over the defect mole fraction is illustrated in Figure 5-13. In this figure, the free energy change associated with creation of a defect is illustrated as a function of the defect mole fraction (N=1). A defect mole fraction at the minimum of system free energy change (ΔG) is the mole fraction at equilibrium. α is equal to the slope of ΔG (equation (14)).

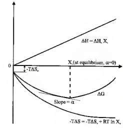

Figure 5-13 Free energy change versus defect concentration.

Assumptions were made in order to understand the term α as it relates to the MBE growth of AlN Si. First, MBE growth of AlN is a non-equilibrium process, during which a meta-stable state of the material can exist. This is particularly true for low temperature MBE growth, during which diffusion of the unincorporated surface atoms is limited, preventing then from reaching equilibrium. Also under carefully chosen growth conditions, the formation of specific defects can be encouraged or discouraged, which will increase the magnitude of the non-equilibrium factor (α)

Secondly there are fewer charged aluminum vacancies in the material than under equilibrium situations. Therefore the driving force to equilibrium is the formation of charged vacancies in order to reduce the total free energy of the system. This is an important assumption since it defines the sign of α in equation (14). This assumption will be valid for growth conditions where aluminum vacancy formation is suppressed. Under such condition, the sign of α is negative since the free energy of the system will only decrease as the concentration of charged vacancies increases. If the system is farther from equilibrium in this direction, the value of α will be more negative increasing the value of $(\Delta G_i^f - \alpha)$ in equation (17). As a consequence, the concentration of the compensating charged defect (n) will decrease. For example, decreasing the AlN growth temperature or adding Ga flux will reduce any group III vacancy (V_{Al}) compensation by encouraging the incorporation of group III elements.

A theoretical calculation of the exact value of the non-equilibrium factor (α) however, is extremely difficult because it is hard to define how much the system parameters influence the value. For example, temperature is one such parameter that influences the value of α. It is expected that the value of α will be more negative the farther the growth temperature is below the equilibrium temperature. However the magnitude of the effect will depend on the separate energy values of formation enthalpy (H_v^f) and entropy (S_v^f). Only the total formation energy values, with no temperature dependence was available in the literature. Furthermore, other growth conditions can influence the value of α such as substrate preparation, nitridation conditions, the selection of a buffer layer, total group III flux / nitrogen ratio. In that perspective, α can be even insensitive to the temperature change. The influence of such parameters on the electrical properties of undoped GaN epilayers (Chapter 3, and Chapter 4) was already demonstrated. Assuming the formation of charged nitrogen vacancies is responsible for the free carriers in unintentionally-doped GaN epilayers, a similar strong influence can be expected for AlN epilayers, which makes it difficult to formulate the value of α.

Therefore experimental data obtained in this work was used to estimate the value of α. Figure 5-4 shows a significant change in resistivity values over the growth temperature range 850 to 940°C. In the figure, a temperature of 900°C is expected to be the temperature at which the transition from conducting to insulating material occurs. A lowest resistive value was chosen to estimate the uncompensated free electron concentration assuming a single digit electron mobility, and it is estimated to be 10^{17} - 10^{18} cm^{-3}. A variety of α values were tested using equation (17) to fit the experimental data. Figure 5-14 is the result obtained for α = -1.6 eV. The y-axis values are three times the values of calculated aluminum vacancy concentrations, since each charged vacancy compensates three free electrons. The result explains well the experimental data. Total

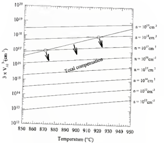

Figure 5-14 Calculated compensating concentration versus temperature plot for AlN with various free electron concentrations (non-equilibrium factor (α) = -1.6eV)

compensation is expected for free electron concentrations below ~ 3 x 10^{16} cm^{-3} in the temperature range A transition temperature of ~ 900°C was expected for the samples having an original free electron concentration of ~ 4 x10^{17} cm^{-3} If the value of α is temperature dependent, as the growth temperature decreases the magnitude of α will increase (become more negative) Therefore, the slope of a line in Figure 5-14 which indicates insulating-to-conducting transition, will become steeper

Kinetic Considerations

Interaction between the growing surface and the molecular beams was considered in order to explain the Si incorporation change with introduction of a Ga flux (Figure 5-9) Epitaxial growth of III-V nitrides in the (0001) direction progresses by the deposition of alternating layers of each group element, as illustrated in Figure 5-15 This model first assumes a perfect growth front, terminated with nitrogen, then the initial adsorption of species followed by competing species that compete for site occupancy Although the atoms or molecules of the various beams arrives together and at random, planar epitaxial growth, under stochiometric conditions will progress in the manner considering the final alternate layer structure

For Si-doping of AlN (the case without a Ga flux), the relative flux ratio of Al:Si used was 1000 1 The growth temperature range of 850 - 940°C was much lower than the temperatures of the Al, and Si effusion cell temperatures (1150, and 1280°C, respectively) Therefore, if the reactivities to the nitrogen of the arriving elements are to be the same the flux ratio of 1000 1 is expected to be maintained in the growing film.

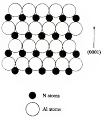

Figure 5-15 Cross sectional view of Wurtzite III-V nitride structure

However, Al is determined to be a reducing agent for Si,[44] meaning that the concentration of Si incorporated into the AlN epilayer is expected to be less than predicted from the flux ratio. Therefore, Al will dominate over Si in occupying the available sublattice sites as illustrated in Figure 5-16. It was determined by SIMS analysis in this work (Figure 5-2, 5-3, and 5-4) that the reducing effect of Si by Al is not sensitive to the AlN growth temperature in the range studied. Also, the Al sticking coefficient was constant over the temperature range studied as evidenced by the AlN growth rate remaining fixed.

The influence of the presence of a Ga flux on Si and Al incorporation is now considered. Silicon is expected to dominate over Ga in the competition to occupy group III sublattice sites because experience has shown that Si is easily incorporated into GaN.[21] Furthermore, GaN becomes thermodynamically unstable under the pressure (1×10^{-5} Torr) and temperature range (850 ~ 940°C) used in this work while AlN is expected to be stable up to ~2000°C.[45] The equilibrium vapor pressure of Ga at the growth temperature is also high (~10^{-2} Torr), predicting a short Ga residence time at the surface. From these considerations, it is also expected that Al will preferably occupy the sublattice sites over Ga. The low Ga content (compared to the relative Ga and Al fluxes used) in the films verifies this prediction (see Figure 5-8). Temporarily adsorbed Ga atoms can provide sites for Si and Al incorporation. Especially for Si, the probability of incorporation will be greater than that of the case without a Ga flux, as illustrated in Figure 5-16, and 5-17. Such an increased incorporation of Si was evidenced by the SIMS data presented earlier (see Figure 5-9).

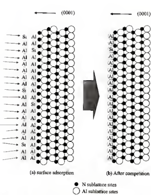

(a) surface adsorption

(b) After competition

Figure 5-16 Site occupancy development during growth of Si-doped AlN (without a Ga flux)

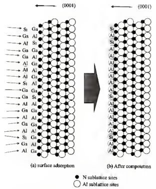

(a) surface adsorption

(b) After competetion

● N sublattice sites

○ Al sublattice sites

Figure 5-17 Site occupancy development during growth of Si-doped AlN (with Ga flux)

The increase in incorporated Si can result in a transition from insulating to conducting material. According to the non-equilibrium model (Figure 5-14) an increase in the free carrier concentration will increase the conducting-to-insulating transition temperature by suppressing compensating defect formation. This explains the resistivity changes brought on by the presence of Ga flux (Figure 5-8).

CHAPTER 6
SUMMARY AND CONCLUSIONS

The following conclusions are drawn from this research.

1. By performing a systematic investigation of *ex vacuo* and *in situ* surface preparation procedures, methods to obtain atomically smooth and clean sapphire surfaces (RMS for 5 x 5 μm AFM scan ~ 1Å) were developed. Standard solvent cleaning followed by acid etching in a H_2SO_4 : H_3PO_4 (3:1) solution at 160°C was used for the *ex vacuo* surface preparations. An acid etching time of at least 90 minutes is needed to remove the sapphire surface polishing damages. GaN films grown on such prepared surfaces were determined to be superior in electrical properties to the films grown on the substrates cleaned using a shorter time. *In situ* heating up to 940°C was needed to obtain a clear sapphire surface RHEED pattern. At least a 60-minute thermal cleaning time at 940°C was required for completion of AlN layer formation during nitridation.

2. Optimized sapphire nitridation conditions were developed using RHEED and AFM analyses. A complete formation of AlN on the sapphire surface was observed after a 120-minute nitridation at 940°C, employing nitrogen free-radical source conditions as follows: a rf forward power of 250W and a nitrogen pressure of 1×10^{-5} Torr. Various stages of nitridation were compared by growing GaN epilayers on such prepared surfaces, and the best electrical properties were obtained from films grown on completely nitrided surfaces.

3. A high temperature (900°C) AlN buffer layer growth procedure was developed and determined to be superior to the conventional commonly used low temperature AlN buffer layer growth procedure for epitaxial nitride growth. Planar (2-D) epitaxial growth was maintained during high temperature AlN buffer layer growth, while layers deposited at low temperature (750°C) were amorphous until annealed at higher temperatures. Much smoother surfaces were obtained for AlN buffer layers grown at directly at 900°C. Furthermore, undoped GaN layers grown on high temperature AlN buffers were insulating while those grown on low temperature buffers were conducting.

4. Low temperature (down to 850°C) epitaxial AlN growth was demonstrated by appropriate selection of growth conditions. Also, $Al_xGa_{1-x}N$ ($x \geq 0.75$) was grown by supplying a Ga flux at various temperatures (850 - 940°C). All undoped $Al_xGa_{1-x}N$ epilayers were insulating.

5. Conducting (conductivities as high as 17 Ω^{-1}-cm^{-1}) $Al_xGa_{1-x}N$ ($x \geq 0.75$) epilayers were produced for the first time by Si-doping. The influence of growth parameters, such as growth temperature, and the addition of a Ga flux, on the conductivity was studied. Conductivity values increased with decreasing growth temperature and also with the addition of a Ga flux.

6. A non-equilibrium model was developed after considering the thermodynamics and kinetics. The model was based on free carrier compensation by charged native vacancies, and predictions from the model were matched with the experimental observations.

It is concluded that compensation by the formation of charged vacancies is the main reason for the difficulty in obtaining conducting AlN and high Al-content AlGaN and by suppressing the formation of compensating charged vacancies in a non-equilibrium growth environment, conducting $Al_xGa_{1-x}N$ ($x \geq 0.75$) epilayers can be obtained through intentional doping. A non-equilibrium growth environment was apparently established in this work when growth temperatures less than 900°C were employed.

It is also important to carefully control growth procedures to produce an appropriate environment for growing conducting $Al_xGa_{1-x}N$ ($x \geq 0.75$) epilayers.

Gallium is a good surfactant element that encourages Si dopant incorporation in AlN and high Al-content AlGaN by providing favorable Al sublattice sites for Si to be incorporated.

LIST OF REFERENCES

1. S Nakamura, T Mukai, and M. Senoh, Appl. Phys Lett. 64, 1687 [1994]
2. S Nakamura, Proc. of the SPIE V2693, 43 [1996]
3. M A Khan, Q Chen, M S Shur, B T Dermott, J A. Higgins, J. Burm, W Schaff, and L F Eastman, Electronic Letters 32, 357 [1996]
4. Y F Wu, B P Keller, S Keller, D Kapolnek, P Kozodoy, S P Denbaars, and U K. Mishra, Appl Phys Lett 69, 1438 [1996]
5. S C. Binari, J M Redwing, G Kelner and W Kruppa, Electronic Letters 33, 242 [1997]
6. Q Chen, R. Gaska, M. Asif Khan, M.S Shur, A. Ping, I Adesida, J Burm, W.J Schaff, and L.F Eastman, Electronic Letters 33, 637 [1997]
7. G R. Kline, and K.M Lakin, Appl. Phys. Lett 43, 750 [1983]
8. M C Benjamin, C Wang, R.F Davis, and R. J Nemanich, Appl Phys. Lett. 64, 3288 [1994]
9. T.L Chu, D W Ing, and A.J Noreika, Solid State Electron. 10, 1023 [1967]
10. X Zhang, P Kung A. Saxler, D Walker, T C. Wang, and M. Razeghi, Appl. Phys Lett 67, 1745 [1995]
11. M D Bremser W G Perry, T Zheleva, N V Edwards, O H Nam, N Parikh, D.E Aspnes, and R.F Davis, MRS Internet Journal Vol. 1, Article 8 [1996]
12. Y Ohda, and A. Hatano, Jpn, J Appl. Phys. V35, L1013 [1996]
13. K. Wefers, and C Misra, in " Oxides and Hydrooxides of Aluminum", Alcoa Laboratories, p31 [1987]
14. T Sasaki, and S Zembutsu, J Appl. Phys. 61, 2533 [1987]
15. H Liu, J G Kim, H. Ludwig, and R.M. Park, Appl. Phys Lett. 71, 347 [1997]

16. M Yeadon, W Kim, A.E. Botchkarev, S N Mohammad, H Morkoc, and J.M. Gibson, MRS Symp Proc. V449 239 [1997]

17. P.S P Wei, and A.W Smith, J Vac Sci. and Technol. 9, 1209 [1972].

18 J M Chang, Appl. Phys. Lett 10 139 [1967]

19 C C. Chang, J. Appl. Phys. 39 5570 [1968]

20 T M. French, and G A. Somorjai, J of Phys. Chem. 74, 2489 [1970]

21 S D Hersee, J Ramer, K. Zheng, C Kranenberg, K. Malloy, M Banas, and M Goorsky J of Electronic Materials 24, 1519 [1995]

22. S Sasaki, and T Matsuoka, J. Appl. Phys. 77, 192 [1995]

23 T W Weeks, Jr , M.D Bremser, K. Shawn Ailey, E. Carlson, W G Perry, and R.F Davis, Appl. Phys Lett. 67, 401 [1995]

24 K. Kawabe, R.H Tredgold, and Y Inuishi, Elect Eng Jpn. 87, 62 [1967]

25 J Edwards, K. Kawabe, G Stevens, and R.H. Tredgold, Solid State Commun. 3, 99 [1965]

26. R.F Rutz, Appl. Phys Lett 28, 379 [1976]

27 C R. Abernathy, S.J Pearton, J.D Mackenzie J W Lee, C.B Vartuli, R.G Wilson, R.J Shul, J.C Zolper and J M. Zavada, MRS Symp Proc V395 685 [1996]

28 P Stumm, and D A. Drabold, MRS Symp Proc V468, 111 [1997]

29 C Stampfl, and C G Van de Walle, Appl Phys Lett 26, 459 [1998]

30 C. Wetzel, T Suski, J W. AgerIII E R Webber E E Haller S Fischer, B K. Meyer, R.J Molnar and P Perlin, Phys. Rev Lett 78 3923 [1997]

31 T Mattila, and R.M Nieminen, Phys. Rev B 54 16676 [1996]

32 L Ungier and J R. Arthur, H M Yoo, and T G Stoebe, J Vac Sci and Technol. B 10, 1226 [1992]

33. R.M. Park, J Vac. Sci. and Technol. A 10, 701 [1992]

34 H Liu, A.C Frenkel, J G Kim, and R.M. Park, J Appl. Phys. 74 6124 [1993]

35 J G Kim, A.C Frenkel, H. Liu, and R.M Park, Appl. Phys Lett 65, 91 [1994]

36 S E Hooper, C T Foxon, T S Cheng, L C Jenkins, D E. Lacklison, J W Orton, T Bestwick, A. Kean, M Dawson, and G Duggan, J Cryst Growth 155, 157 [1995].

37 N A. Burnham, and R.J Colton, J Vac. Sci and Technol. A 7, 2906 [1989]

38 N A Burnham, and R J Colton, in Scanning Tunneling Microscopy Theory and Practice. (D A. Bonnell, ed.) V C H. Publishers, New York [1991]

39 L.J Van der Pauw Philips Res Repts. 13, 1 [1958]

40 W.J Bartels, J Vac Sci and Technol B 1, 338 [1983]

41 J.I Goldstein, D E Newbury, P Echlin, D C. Joy, C.E Fiori, and E Lifshin, Scanning Microscopy and X-ray Microanalysis. Plenum, New York [1981]

42 D E Newbury D C Joy P Echlin, C E Fiori, and J I Goldstein. Advanced Scanning Electron Microscopy and X-ray Microanalysis. Plenum, New York [1986]

43 T.L. Tansley, and R.J Egan, Phys. Rev B 45 10942 [1992]

44 D P Griffis, R. Loesing, D.A. Ricks, M C Bremser, and R.F Davis, SIMS VI 201 [1998]

45 I. Grzegory J. Jun, St. Krukowski, M. Bockowski, and S Porowski, Physica B 85, 99 [1993]

BIOGRAPHICAL SKETCH

Jongim George Kim was born on February 18, 1969, in Seoul, Korea. He attended Hong-Ik University, Seoul, Korea and earned a Bachelor of Science degree in Metallurgical and Materials Engineering in February 1991. Upon graduation, he was awarded a Student of the Year award by the Engineering College for graduating with the highest GPA among the all of the graduates in the University.

After graduating, he decided to study in the United States and to take graduate courses in electronic materials. In spring 1992, he was admitted to the Department of Materials Science and Engineering at University of Florida. In the summer of 1992, he joined Dr. Robert M. Park's III-V MBE research group working on the development of wide bandgap semiconductor materials. He received his Master of Science degree in Materials Science and Engineering in the spring of 1994. His master's thesis detailed his research work on the MBE growth and electrical properties studies of Si-doped, cubic phase GaN.

In the fall of 1994, he entered the Ph.D program in the Department of Material Science and Engineering at the University of Florida and continued studying the group III nitride system. He maintained high academic standards (cumulative GPA 4.0/4.0) throughout the graduate study in the United States. He also authored or co-authored 6 journal publications during his graduate research.

I certify that I have read this study and that in my opinion it conforms to acceptable standards of scholarly presentation and is fully adequate, in scope and quality, as a dissertation for the degree of Doctor of Philosophy

Robert M. Park

Robert M. Park, Chairman
Professor of Materials Science
and Engineering

I certify that I have read this study and that in my opinion it conforms to acceptable standards of scholarly presentation and is fully adequate, in scope and quality, as a dissertation for the degree of Doctor of Philosophy

R. E. Hummel

Rolf E. Hummel
Professor of Materials Science
and Engineering

I certify that I have read this study and that in my opinion it conforms to acceptable standards of scholarly presentation and is fully adequate, in scope and quality, as a dissertation for the degree of Doctor of Philosophy

Sheng S. Li
Professor of Electrical and Computer
Engineering

I certify that I have read this study and that in my opinion it conforms to acceptable standards of scholarly presentation and is fully adequate, in scope and quality, as a dissertation for the degree of Doctor of Philosophy

Joseph H. Simmons
Professor of Materials Science
and Engineering

I certify that I have read this study and that in my opinion it conforms to acceptable standards of scholarly presentation and is fully adequate, in scope and quality, as a dissertation for the degree of Doctor of Philosophy

Rajiv K. Singh
Professor of Materials Science
and Engineering

This dissertation was submitted to the Graduate Faculty of the College of Engineering and to the Graduate School and was accepted as partial fulfillment of the requirements for the degree of Doctor of Philosophy.

August, 1998

Winfred M. Phillips
Dean, College of Engineering

Karen A. Holbrook
Dean, Graduate School